9.11 SENSITIVITY OF CLOUD-RADIATION INTERACTIONS TO CLOUD MICROPHYSICS

Sam F. Iacobellis[*1], Richard C. J. Somerville[1], Greg M. McFarquhar[2], and David Mitchell[3]

[1]Scripps Institution of Oceanography, University of California, San Diego
[2]Department of Atmospheric Sciences, University of Illinois at Urbana-Champaign
[3]Division of Atmospheric Sciences, Desert Research Institute

1. INTRODUCTION

Unrealistic parameterizations are the Achilles' heel of climate models. When a single-column model (SCM), which consists of one isolated column of a global atmospheric model, is forced with observational estimates of horizontal advection terms, the parameterizations within the SCM produce time-dependent fields which can be compared directly with measurements. In the case of cloud microphysical schemes, these fields include cloud altitude, cloud amount, liquid and ice content, particle size spectra, and radiative fluxes at the surface and the top of the atmosphere. Comparisons with data from the Atmospheric Radiation Measurement (ARM) Program show conclusively that prognostic cloud algorithms with detailed microphysics are far more realistic than simpler diagnostic approaches. Long-term comparisons of quantities strongly modulated by clouds, such as monthly mean downwelling surface shortwave radiation, clearly demonstrate the superiority of parameterizations based on comprehensive treatments of cloud microphysics and radiative interactions. These results also demonstrate the critical need for more and better in situ observations of cloud microphysical variables.

We have used an SCM to examine the sensitivity of fundamental quantities such as atmospheric radiative heating rates and surface and top-of-atmosphere radiative fluxes to various parameterizations of clouds and cloud microphysics. The single-column model was run at the ARM Southern Great Plains (SGP), Tropical Western Pacific (TWP), and North Slope of Alaska (NSA) sites using forcing data derived from operational numerical weather prediction. Our results indicate that atmospheric radiative fluxes are sensitive to the scheme used to specify the ice particle effective radius by up to 30 Wm^{-2} on a daily time scale and up to 5 $W m^{-2}$ on a seasonal time scale. We also found that the inclusion of ice particle fallout can have a significant effect on the amount and location of high cirrus clouds. On a seasonal time scale, atmospheric fluxes were sensitive to the inclusion of ice particle fallout by 8 $W m^{-2}$. An unexpected finding was that the variance of the modeled ice particle effective radius at a given level is considerably smaller than that suggested by ARM cloud radar measurements. Our results indicate that this theoretical underestimate of the ice particle effective radius variance can have effects on modeled radiative fluxes comparable in magnitude to those cited above for sensitivity to the mean values of ice particle effective radius.

* Corresponding author address: Sam F. Iacobellis, Scripps Institution of Oceanography, La Jolla, CA 92093-0224; e-mail: siacobellis@ucsd.edu.

2. MODEL DESCRIPTION

The SCM represents an isolated column of atmosphere extending upwards from, and including, the underlying surface. Unlike a three-dimensional general circulation model (GCM), the isolated atmospheric column within the SCM does not have any horizontally adjacent columns. As a result, time-dependent horizontal advective fluxes of heat, moisture and momentum (used to derive vertical velocity) must be supplied to SCM.

The necessary forcing data for the SCM was obtained from a version of the National Center for Experimental Predictions (NCEP) Global Spectral Model (GSM) (Roads et al, 1999). The forcing data was produced using the 0 - 24 hour fields from each daily forecast made by the GSM. These individual 24-hour forecasts were concatenated to produce a continuous forcing data set that extends back to May 2000. The SCM was run at the ARM SGP, TWP, and NSA sites using this forcing data. Additionally, a 3-month subset (JJA 2000) of this forcing data was used to run the SCM at the SGP site to examine model sensitivities to the specification of cloud microphysics. In addition to the horizontal advective fluxes of heat, moisture and momentum, the surface temperature and surface heat fluxes were also specified from the GSM forecast products.

The SCM utilizes 53 layers (Iacobellis and Somerville, 2000) and thus has a relatively high vertical resolution (Lane et al, 2000). The horizontal extent represents a single column of a GCM centered on the each of the ARM sites. The SCM incorporates relaxation advection (Randall and Cripe, 1999) to keep the modeled temperatures and humidities from drifting towards unrealistic values.

3. RESULTS

3.1 Long-term Analysis of SCM Control Version

The control SCM run (CONTROL) utilized a prognostic cloud parameterization (Tiedtke, 1993) together with interactive cloud optical properties for both liquid (Slingo, 1989) and ice (McFarquhar, 2002a) clouds. The effective radius is also calculated interactively using the schemes of Bower et al (1994) for liquid droplets and McFarquhar (2001) for ice particles. Ice particle settling is included in the SCM with individual crystal fall speeds calculated from Mitchell (1996).

Typical fall speeds range from 0.25 to 1.0 m sec^{-1}. Maximum cloud overlap has been assumed throughout this study.

Figure 1 shows the monthly mean downwelling surface shortwave radiation (DSSR) from the SCM, the GSM and ARM surface observations at each of the three ARM sites for the period May 2000 to June 2002. At all three sites, the SCM results generally compare very favorably with the ARM surface observations. An exception to this favorable comparison occurs at the TWP site between December 2001 and June 2002. Interestingly, the SCM results compare much better with the observations than the results from the GSM. Analysis indicates that these flux differences are due to the cloud fields produced by each model. This version of the GSM utilizes diagnostic cloud-radiation parameterizations that appear to be inferior to the prognostic cloud scheme with interactive cloud radiative properties used in the SCM.

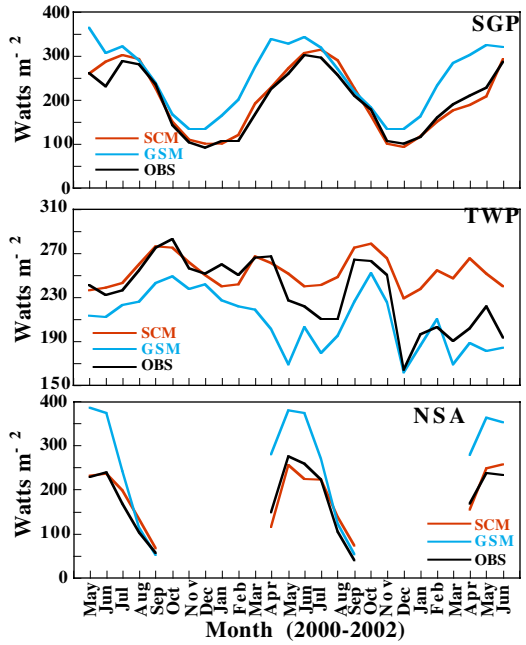

Figure 1. Monthly mean downwelling surface shortwave radiation from the SCM, GSM and surface observations at each of the three ARM Program sites.

3.2 Three month Control Run at SGP Site

Most of the comparisons between model data and observations in this study are performed using averages over the entire 3-month model run. However, it is important to know whether the SCM produces a realistic evolution of model variables using the prescribed forcing data set. The time series of downwelling surface shortwave radiation, TOA shortwave cloud forcing, outgoing longwave radiation (OLR), TOA longwave cloud forcing, cloud fraction, cloud optical thickness, and precipitation from the SCM control run and from ARM and GOES satellite observations are shown in Figure 2. Overall, the model results appear to reproduce much of the observed temporal variability. The model is more successful at capturing the observed trends on longer timescales of 3-4 weeks than at the shorter timescales of a few days to a week. Comparison between modeled and observed cloud fraction, cloud optical thickness, and the four radiative flux variables shown in Figure 2 produced correlation coefficients ranging from 0.63 to 0.89 for 5-day means and 0.50 - 0.69 for daily means. Correlation coefficients of 0.54 (5-day means) and 0.30 (daily means) were obtained from a comparison of modeled and observed surface precipitation.

Cloud fraction results from the SCM are shown along with observational estimates of cloud fraction from both GOES satellite and ARM Millimeter Cloud Radar (MMCR) measurements. The MMCR estimates produce a larger mean cloud fraction (49%) than the GOES satellite data (40%). Most of this difference is probably due to the MMCR measurements detecting high thin cirrus clouds that are beneath the optical thickness threshold of the GOES satellite data. Other differences between the two observational estimates of cloud fraction may be attributed to the MMCR measuring the frequency of cloud occurrence at a single location within the SCM domain while the GOES satellite views the entire domain. The differences between the SCM and either the GOES or MMCR data are comparable to the difference between the two observational estimates.

3.3 Effect of Ice Particle Fallout

An experiment model run (NOFALL) was performed where the ice particle fallout mechanism of Mitchell (1996) was removed. As one would expect, the removal of ice particle fallout increased the amount of high clouds, as illustrated in Figure 3. Without the removal of ice particles from these layers, the clouds that formed existed for longer times.

The ice crystal fall speed calculation (Mitchell, 1996) used in CONTROL assumed a planar-polycrystal ice crystal habit. Additional runs were performed that included ice particle fallout using hexagonal columns, bullet rosettes, and spheres as the assumption of crystal habit. The 3-month mean values of several parameters were calculated from these three additional runs and CONTROL. Table 1 shows the difference of these mean values from those calculated in model run NOFALL (no ice particle fallout) along with the mean ice particle fall speed for each assumed crystal habit. The sensitivity of the model results to the assumption of ice habit can be examined by comparing the values between each run. The mean ice crystal fall speed from these experiments varied from a low of 0.42 m sec^{-1} (spheres) to a high of 0.74 m sec^{-1} (rosettes). Not surprisingly, the mean cloud amount decreased as the mean ice crystal fall speed increased. The runs which included ice particle fallout produced higher values of IWP than model run NOFALL. One might expect to see a decrease in the IWP when ice crystal fallout is activated. However, feedbacks within the SCM act to increase the convective mass flux and ice water detrainment which more than offsets any loss of ice water due to settling. It is not clear if this result is dependent on the particular SCM used in this study.

Crystal Habit	Mean Fall Speed (m s^{-1})	Cloud Amount	Cloud Height	IWP	OLR	DSSR
NOFALL						
Polycrystals	0.61	-12.3	-2.7	7.8	3.4	0.0
Columns	0.47	-11.2	-2.4	7.4	2.9	0.1
Rosettes	0.74	-14.4	-2.8	6.5	4.1	0.1
Spheres	0.42	-10.1	-1.8	4.5	2.6	0.1

Table 1. Mean values of selected parameters from CONTROL and three additional runs using a different assumption of ice crystal habit in calculating the ice crystal fall speed. The mean fall speeds are presented in units of m sec^{-1} while all other quantities are percentage difference from model run NOFALL.

Interestingly, the change in cloud amount did not result in any significant change in mean DSSR (< 1 W m^{-2}). There are two factors to explain the non-varying DSSR. First, the larger IWP resulted in higher cloud optical thicknesses which partly compensated for the reduced cloud amount. However, another contributing factor is due to the mean diurnal pattern of increased cloud fraction in NOFALL. Figure 4 shows the mean diurnal pattern (overall mean from each run removed) of cloud amount from CONTROL and NOFALL. The increase in the mean cloudiness from NOFALL occurs mostly in the late evening and early morning hours when there is little or no solar radiation. In both runs, convection is dominant in the late afternoon with detraining cloud water/ice forming cirrus anvil clouds that reach a peak magnitude around 1600 local time. Soon after this time, the cloud amount begins to decrease in both runs. However, the cloud amount decreases faster in CONTROL due to ice particle fallout.

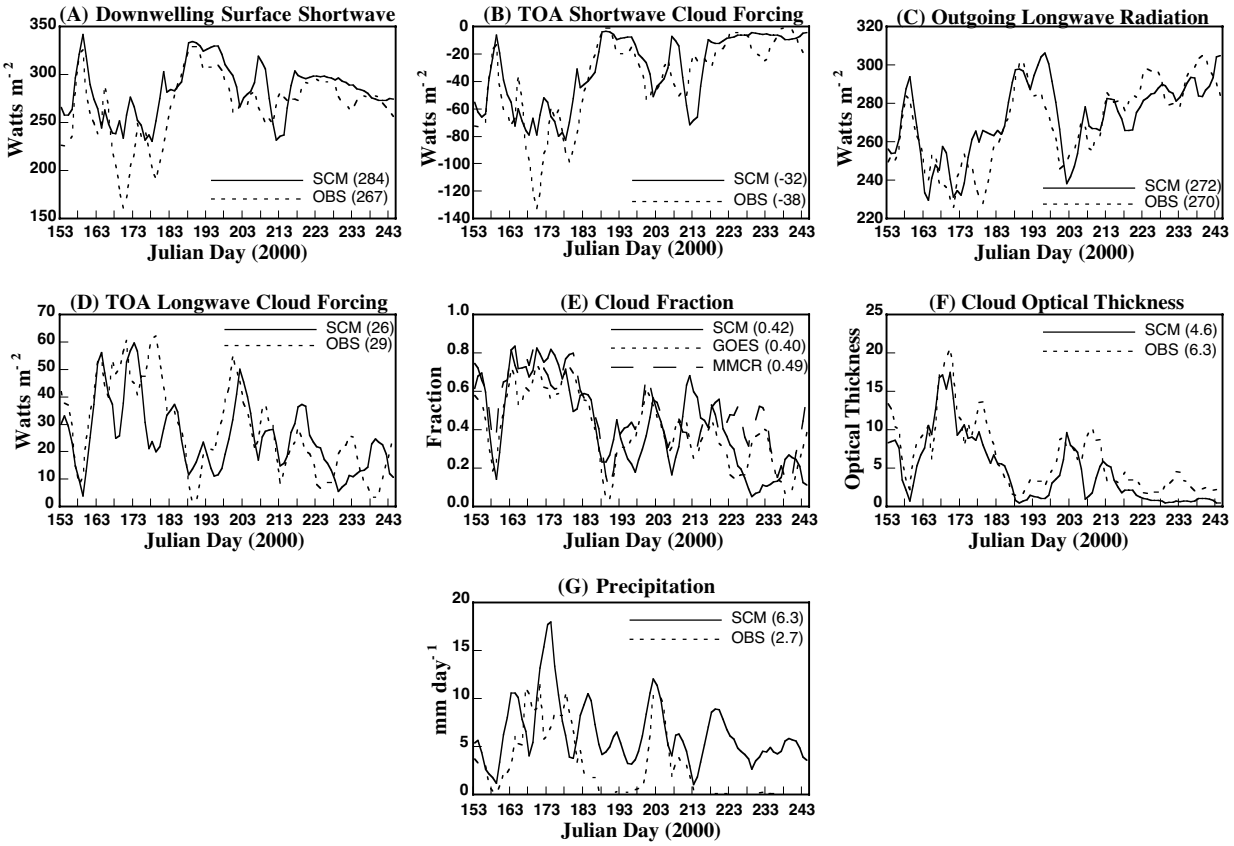

Figure 2. Time series of (a) downwelling surface shortwave radiation, (b) TOA shortwave cloud forcing, (c) outgoing longwave radiation, (d) TOA longwave cloud forcing, (e) cloud fraction, (f) cloud optical thickness, and (g) surface precipitation from the SCM control run (solid line) and from observations (dashed line). Observations of OLR, cloud optical thickness and both cloud forcing terms are from GOES-10 satellite measurements; downwelling surface shortwave radiation and precipitation are from ARM surface measurements; and cloud fraction from both the MMCR and GOES-10 satellite measurements. The numbers in parentheses are the mean values over the entire 3-month integration period. Both the model results and observational data were smoothed using a five-day running mean filter.

The modeled OLR is more sensitive to the inclusion of ice particle fallout and the assumption of ice crystal habit than the DSSR. This increased sensitivity arises partly because the diurnal pattern of cloudiness changes noted above will have little effect on the OLR. Furthermore, the data in Table 1 shows that the mean OLR increased as the mean ice crystal fall speed increased. Most of this change is due to the reduction in cloud amount as ice particle fall speed increases. However, part of the change is due to the decrease in the mean cloud height as ice particle fall speeds increase. A lower mean cloud height results in a warmer

effective cloud temperature thereby increasing the emission of longwave radiation by the clouds. Using the mean cloud height, lapse rate and cloud amount from CONTROL, the reduction in cloud height (relative to NOFALL) increased the OLR about 2 W m^{-2} or about 22% of the total increase.

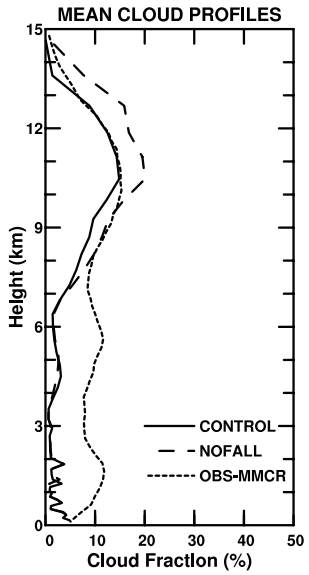

Figure 3. Mean vertical profile of cloud fraction from the control run (solid line), run NOFALL (long-dashed line), and from MMCR measurements (short-dashed line) at the ARM SGP site during the 3-month period JJA 2000.

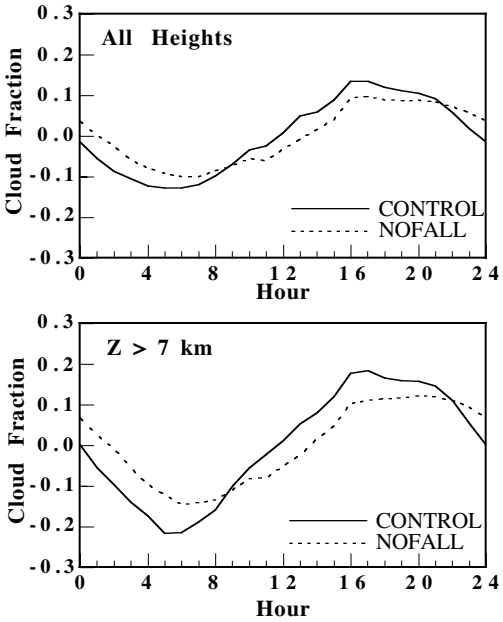

Figure 4. The mean diurnal variation of cloud fraction including all cloud heights (top); and cloud fraction with only clouds above 7 km included (bottom) from the SCM control run (solid line) and from NOFALL (dashed line). Note that the overall mean cloud amount has been subtracted from each curve.

3.4 Effect of Ice Particle Radius Parameterization

The parameterization of the ice particle effective radius used in the control run was replaced with alternate schemes in three additional model runs ICEREWY (Wyser, 1998), ICERESU (Suzuki et al, 1993) and ICEMITC (Mitchell et al, 1996; Ivanova et al, 2001). The fractional cloud amounts produced by these three model runs did not vary significantly from CONTROL. However, these runs produced different mean vertical profiles of ice particle effective radius and consequently different ice cloud optical properties. Figure 5 shows the mean vertical profiles of ice particle effective radius from these model runs and from the ice cloud properties data set of Mace et al (1998, hereafter M98). The M98 data set uses an algorithm that combines MMCR cloud reflectivity data with co-located infrared radiance data. The technique described in McFarquhar et al (2002b) was used to convert the various definitions of effective particle radius encountered in this study to Fu's (1996) definition of R_{eff} for comparison purposes. The mean R_{eff} from all four model runs decreases with increasing height as does the observational data. While the profiles from CONTROL and ICEMITC are similar, there are still notable differences between these two profiles and those from ICEREWY and ICERESU, and it is difficult to determine which compares most favorably with the observational data. The wide range of mean R_{eff} profiles is not entirely unexpected. Each of the R_{eff} schemes is based upon a different set of in situ measurements with varying assumptions about the ice crystal habits.

Some of the SCM runs in this study use schemes that parameterize R_{eff} as a function of temperature and ice water content. Obviously, these schemes cannot be expected to produce a realistic value of R_{eff} if the model ice water content is unrealistic. Figure 6 displays the mean vertical profile of cloud temperature and cloud ice water content from the control run and from the M98 ice cloud properties data set. The mean profiles of temperature and ice water content from each of the four runs are nearly identical and only the control run is displayed for clarity. The modeled cloud ice water content compares reasonably well with the measured values in the middle troposphere below roughly 9 km, but begins to underestimate the measured values significantly as one moves towards the tropopause. As a result, errors in the SCM values of R_{eff} above 9 km may be due to the model underestimating the ice water content.

However, some of this difference in IWC may be due to errors in the predicted particle size distribution used by the algorithm of the M98 data set. The algorithm is particularly insensitive to small particles and the small particle distribution is predicted based on the observed distribution of larger particles. This can lead to serious errors in the small particle distribution as noted by M98. If the M98 algorithm underestimated the number of small particles, a larger value of IWC would be predicted in order to produce a cloud emissivity to match the measured value. In addition, one would expect the number of small particles, and hence their relative influence on the cloud radiative properties, to increase

as the altitude increases between 9 and 15 km. This may help explain the differences between SCM and measured IWC above 9 km.

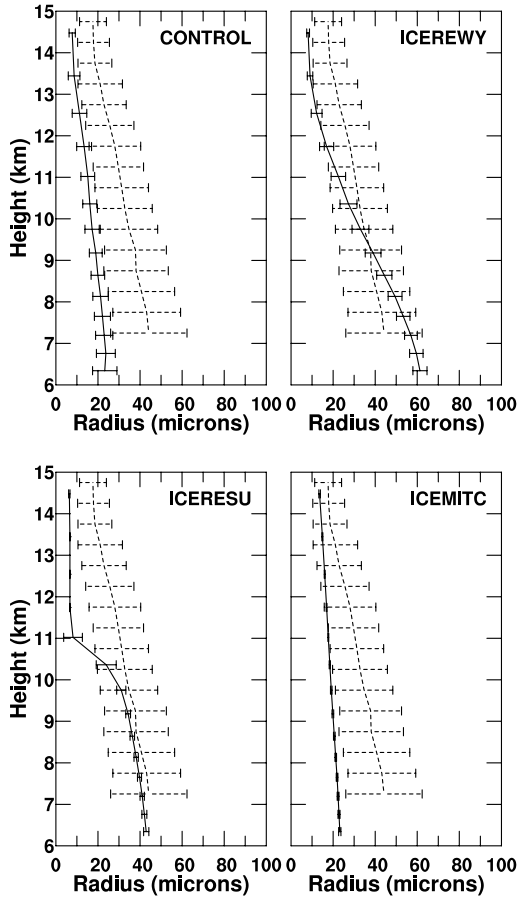

Figure 5. Mean vertical profiles of ice particle effective radius from the SCM control run and from runs ICEREWY, ICERESU and ICEMITC. The model results are shown by the solid lines and the dashed lines denote the values from the Mace et al (1998) ice cloud properties data set for the corresponding period. The width of the horizontal bars is equivalent to +/- _(z), where _(z) is the standard deviation at each level.

All four SCM runs underestimate R_{eff} above 9 km which is what one would expect if low values of IWC are used. However, the Suzuki et al (1993) parameterization used in ICERESU calculates R_{eff} as a function of temperature only indicating that the discrepancies above 9km may be due to more than just low values of modeled IWC. Below 9 km where the model produces reasonable estimates of ice water content, two of the four SCM runs (ICEREWY and ICERESU) produced mean values of R_{eff} within the standard deviation of the observed data.

Hourly means values of model and measured data were examined in order to determine whether errors in the SCM IWC are responsible for the underestimates of R_{eff} noted above. In order to isolate those times when the SCM values of IWC and cloud temperature were in close agreement with measured values, the following criteria were used to select of subset of hourly means: i) those hours when the SCM cloud fraction maximum occurred within the cloud base and cloud top limits indicated by the M98 data; and ii) hours when the SCM IWC was within 50% of the M98 value. Application of these criteria resulted in approximately 20-25 hourly means for each SCM experiment. The top two rows of Figure 7 show the M98 values of IWC and cloud base temperature plotted against the SCM values from experiments CONTROL, ICEREWY, ICERESU, and ICEMITC for those hourly means that satisfied the above criteria. The bottom row in Figure 7 shows the value of R_{eff} from the M98 data set plotted against the SCM value for each of the four experiments. This information in Figure 7 shows that even when the IWC and cloud temperature are close to the measured values, the SCM and the M98 values of R_{eff} still do not agree well. That is, it does not appear that the differences between the SCM and M98 values of R_{eff} are due to errant values of model calculated IWC. The R_{eff} parameterizations used in CONTROL (McFarquhar, 2001) and ICEMITC (Ivanova et al, 2001) were both based on ice particle distributions that had dedicated instrumentation to measure small ice particles. It is not surprising that these two experiments predict a larger contribution from small particles, as evidenced by the lower values of R_{eff}, than either ICEREWY (Wyser, 1998) or ICERESU (Suzuki et al, 1993). These results are consistent with either the M98 data underestimating or the McFarquhar (2001) and Ivanova et al (2001) schemes overestimating the contributions of small ice particles.

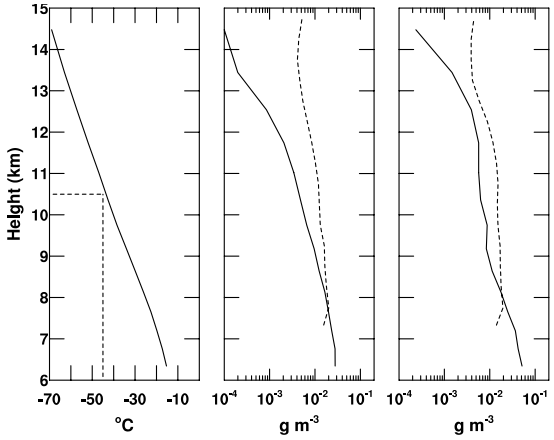

Figure 6. Mean vertical profile of cloud temperature, ice water content and ice water content standard deviation from the SCM control run (solid lines). The dashed lines in panel (a) indicate the height of the -45°C level while the dashed lines in panels (b) and (c) represent the ice water content and ice water content standard deviation from the Mace et al (1998) ice cloud properties data set (dashed lines).

A feature of the Ivanova et al (2001) scheme contained in the SCM is that one can specify the crystal habit and the distribution shape (monomodal vs. bimodal). The settings in the ICEMITC run specified planar polycrystals and a bimodal particle size distribution. Additional runs were performed using both hexagonal columns and a monomodal distribution. The mean R_{eff} profiles from these additional versions of

ICEMITC (along with the original version of ICEMITC) are shown in Figure 8. Clearly, the best comparison to the M98 measurements is found with the Ivanova et al (2001) scheme using hexagonal columns and a monomodal particle size distribution. However, this favorable comparison may be coincidental if the M98 measurements underestimate the contribution from small particles as is likely to occur if a bimodal distribution was encountered. Again, due to possible errors extrapolating the small particle distribution in the M98 measurements, it is difficult to say with any certainty that any one particular scheme compares best.

The variability of R_{eff} at any given level, as measured by the standard deviation, is underestimated by all four parameterizations examined. The radiative flux parameterizations, both longwave and shortwave, are non-linear and an underestimation of the variability of cloud microphysical properties such as R_{eff} could have important consequences on model calculated mean radiative fluxes. To help quantify the effect that the narrow range of R_{eff} has on the modeled radiative fluxes, the control version of the SCM was rerun with a random ΔR_{eff} added to the model calculated value of R_{eff} (model run EXP-WIDE). This was a conservative procedure such that the mean value of R_{eff} at each model level did not change from the control run. Figure 9 shows the probability distribution of effective particle radius from run EXP-WIDE for clouds occurring from 8-9 km and 12-13 km. The width of the distribution from EXP-WIDE more closely matches, albeit not perfectly, the distribution from the M98 data set.

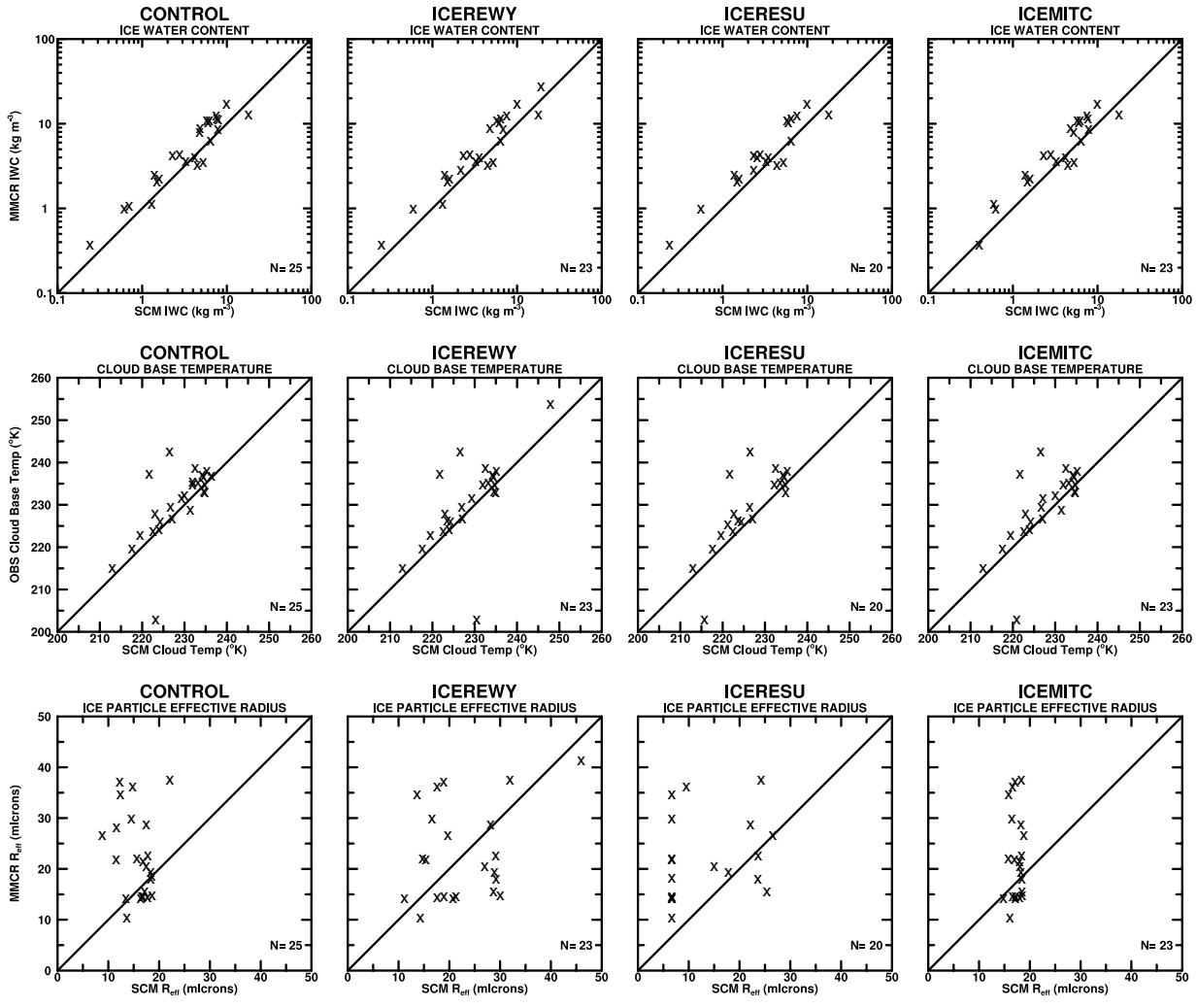

Figure 7. Hourly mean values of IWC (top row), cloud base temperature (middle row), and ice particle effective radius (bottom row). Data from the M98 data set are plotted against a subset of results from model runs CONTROL, ICEREWY, ICERESU, and ICEMITC. The subset of hourly means was chosen such that: i) SCM cloud fraction maximum occurred within cloud base and top limits of M98 data; and ii) SCM IWC was within 50% of the M98 value.

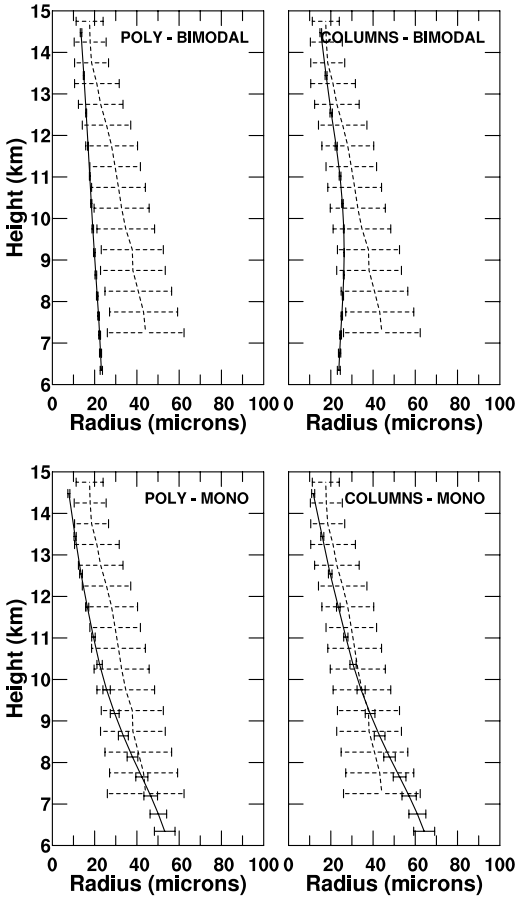

Figure 8. Mean vertical profiles of ice particle effective radius from the SCM using the R_{eff} parameterization of Ivanova et al (2001) with varying assumptions of ice particle habit and distribution shape: a) planar polycrystals and bimodal distribution (ICEMITC); b) hexagonal columns and bimodal distribution; c) planar polycrystals and monomodal distribution; and d) hexagonal columns and monomodal distribution. The model results are shown by the solid lines and the dashed lines denote the values from the Mace et al (1998) ice cloud properties data set for the corresponding period. The width of the horizontal bars is equivalent to +/- $\sigma(z)$, where $\sigma(z)$ is the standard deviation at each level.

The results from model run EXP-WIDE indicate that the change in the distribution of R_{eff} can alter the solar and longwave radiative fluxes at the surface and TOA by up to 5 W m^{-2} relative to the control run. However, at the TOA level it appears that increases in the outgoing solar radiative flux are largely offset by decreases in the outgoing longwave flux resulting in little change in the heat budget for the earth-atmosphere system. The wider distribution of R_{eff} in model run EXP-WIDE results in optically thicker ice clouds (on average) that reflect more sunlight. The optically thicker ice clouds also have a higher mean emissivity compared to the control run thus essentially increasing the effective radiative cloud height and decreasing the outgoing longwave radiation.

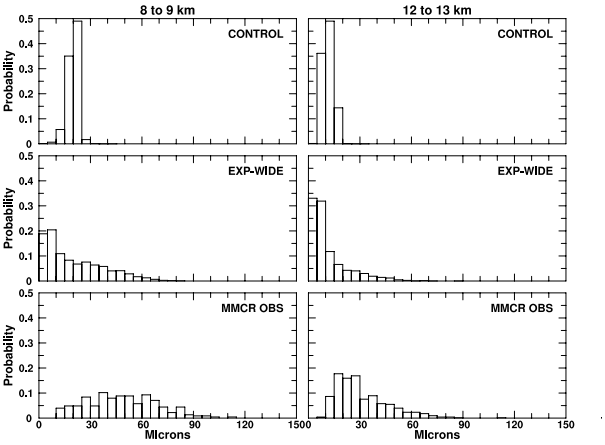

Figure 9. Probability distribution of effective ice particle radius from SCM runs CONTROL and EXP-WIDE. and from ARM MMCR measurements.

ACKNOWLEDGMENTS

This research was supported in part by the Department of Energy under Grant DOEDE-FG03-97-ER62338, the National Oceanic and Atmospheric Administration under Grant NA77RJ0453, the National Aeronautics and Space Administration under Grant NAG5-8292, and the National Science Foundation under Grants ATM-9612764 and ATM-9814151.

REFERENCES

Bower, K. N., T. W. Choularton, J. Latham, J. Nelson, M. B. Baker, and J. Jenson, 1994: A parameterization of warm clouds for use in atmospheric general circulation models. J. Atmos. Sci., **51**, 2722-2732.

Fu, Q., 1996: An accurate parameterization of the solar radiative properties of cirrus clouds. J. Climate, **9**, 2058-2082.

Iacobellis, S. F., and R. C. J. Somerville, 2000: Implications of microphysics for cloud-radiation parameterizations: Lessons from TOGA-COARE. Journal of the Atmospheric Sciences, **57**, 161-183.

Ivanova, D. C., D. L. Mitchell, W. P. Arnott, and M. Poellot, 2001: A GCM parameterization for bimodal size spectra and ice mass removal rates in mid-latitude cirrus clouds. Atmos. Res., **59**, 89-113.

Lane, D. E., R. C. J. Somerville, and S. F. Iacobellis, 2000: Sensitivity of cloud and radiation parameterizations to changes in vertical resolution. Journal of Climate, **13**, 915-922.

Mace, G. G., T. P. Ackerman, P. Minnis, and D. F. Young, 1998: Cirrus layer microphysical properties derived from surface-based millimeter radar and infrared interferometer data. J. Geophys. Res., **103**, 23207-23216.

McFarquhar, G. M., 2001a: Comments on 'Parameterization of effective sizes of cirrus-cloud particles and its verification against observation' by Zhian Sun and Lawrie Rikus (October B, 1999, 125, 3037-3055). Q. J. R. Meteor. Soc., **127**, 261-265.

McFarquhar, G. M., P. Yang, A. Macke, and A. J. Baran, 2002a: A new parameterization of single-scattering solar radiative properties for tropical ice clouds using observed ice crystal size and shape distributions. Submitted to the Journal of the Atmospheric Sciences.

McFarquhar, G. M., S. Iacobellis, R. C. J. Somerville, and G. G. Mace, 2002b: SCM simulations of tropical ice clouds using observationally based parameterizations of microphysics and radiation. Submitted to the Journal of Climate.

Minnis, P., W.L. Smith, Jr., D. P. Garber, J. K. Ayers, and D. R. Doelling, 1995: Cloud properties derived from GOES-7 for the Spring 1994 ARM Intensive Observing Period using version 1.0.0 of the ARM satellite data analysis program. NASA Reference Publication 1366, August 1995, 59 pp.

Mitchell, D. L., 1996: Use of mass- and area-dimensional power laws for determining precipitation particle terminal velocities. J. Atmos. Sci., **53**, 1710-1723.

Mitchell, D. L., A. Macke, and Y. Liu, 1996: Modelling cirrus clouds, part II, Treatment of radiative properties, J. Atmos. Sci., **53**, 2967-2988.

Randall, D. A., and D. C. Cripe, 1999: Alternative methods for specification of observed forcing in single-column models and cloud system models. J. Geophys. Res., **104**, 24527-24546.

Roads, J. O., S.-C. Chen, M. Kanamitsu, and H. Juang, 1999: Surface water characteristics in NCEP global spectral model and reanalysis. J. Geophys. Res., **104**, 19307-19328.

Slingo, A., 1989: A GCM parameterization for the shortwave radiative properties of water clouds. J. Atmos. Sci., **46**, 1419-1427.

Suzuki, T., M. Tanaka, and T. Nakajima, 1993: The microphysical feedback of cirrus cloud in climate change. J. Meteor. Soc. Japan, **71**, 701-713.

Tiedtke, M., 1993: Representation of clouds in large-scale models. Mon. Wea. Rev., **121**, 3040-3061.

Wyser, K., 1998: The effective radius in ice clouds. J. Climate, **11**, 1793-1802.